



Available online at www.sciencedirect.com

ScienceDirect

Procedia Manufacturing 26 (2018) 929–940

Procedia
MANUFACTURING

www.elsevier.com/locate/procedia

46th SME North American Manufacturing Research Conference, NAMRC 46, Texas, USA

Experimental Investigation of Residual Stress and its Impact on Machining in Hybrid Additive/Subtractive Manufacturing

Jarred C. Heigel*, Thien Q. Phan, Jason C. Fox, Thomas H. Gnaupel-Herold

National Institute of Standards and Technology, 100 Bureau Drive, Gaithersburg, MD 20899, USA

* Corresponding author. Tel.: +1-301-975-3620
E-mail address: jarred.heigel@nist.gov

Abstract

Hybrid manufacturing leverages the advantages of both additive manufacturing (AM) with machining to create parts that have complex geometries, tight tolerances, and good surface finish. However, the residual stresses induced by both processes present a challenge. These high stresses can induce significant distortion that can damage the part during the additive process or lead to unanticipated distortion during the machining process. The current work investigates the impact of the residual stresses generated during the AM process on the part distortion during the subsequent machining operation. Laser powder bed fusion is used to create stainless steel cylinders and their geometries are measured before and after machining their outer diameter, allowing the resulting distortion to be calculated. The measured distortion is counter to what is anticipated based on the trends exhibited in the residual stress in the cylinders measured before the machining operation using neutron diffraction. This suggests that the machining process imposes significant stresses that, in this case, counter act the remaining stresses from the AM process and/or trigger a material phase change.

© 2018 The Authors. Published by Elsevier B.V.
Peer-review under responsibility of the scientific committee of the 4th International Conference on System-Integrated Intelligence.

Keywords: Hybrid manufacturing, additive manufacturing, residual stress, distortion

Certain commercial equipment, instruments, or materials are identified in this paper in order to specify the experimental procedure adequately. Such identification is not intended to imply recommendation or endorsement by the National Institute of Standards and Technology, nor is it intended to imply that the materials or equipment identified are necessarily the best available for the purpose. This material is declared a work of the U.S. Government and is not subject to copyright protection in the United States.

1. Introduction

Hybrid additive/subtractive manufacturing is a process that combines both additive manufacturing (AM) and subtractive manufacturing, such as machining, to create parts with high complexity, tight tolerances, and good surface finish [1]. This processing can be done in-envelope, where both AM and machining operations are performed by the same machine [2], or out-of-envelope, where two separate machines are used for each process [3], requiring the part to be moved between each machine. Whichever hybrid approach is used, the AM processing enables complex geometries to be created while the machining creates better geometric accuracy and surface finish than is possible solely using AM [4]. A key difference between the two approaches however, is the ability to manage the residual stresses from the AM process. While the out-of-envelope approach can easily incorporate heat treatments to alleviate the residual stress before machining, the in-envelope approach prohibits intermediate heat treatments. This can be a challenge since the residual stress generated in AM is significant.

AM generates very high residual stresses due to the thermal history imposed by the process [5]. These stresses can cause the part to crack and separate from the build plate or to distort significantly, causing the part to fail or not meet the design requirements. For instance, Denlinger et al. demonstrated through experiment and simulation that the stresses in a 4 m long part fabricated using wire-fed electron beam directed energy deposition (DED) could experience distortion greater than 50 mm [6]. Although simulation can be used to predict the residual stress and distortion so that they can be mitigated or compensated for [7], it is unclear how subsequent machining of the highly-stressed AM material impacts part distortion.

A few studies in the literature have focused on the impact of residual stresses generated during AM on the subsequent machining operations. Lane et al. created stainless steel disks with laser powder bed fusion (LPBF) that were subsequently machined using a turning operation that achieved 2-D orthogonal cutting [8]. A substantial amount of chip curl out of the cutting plane was observed, which was not observed when cutting wrought disks of the same material. This out-of-plane curl was attributed to the residual stress distribution in the disks from the LPBF process, and indicates that residual stresses from the AM process can impact chip formation during machining.

Concerning the impact on geometric error and distortion, Salonitis et al. studied the impact of residual stress and distortion in cylinders created using laser cladding on the subsequent machining operation [9]. Using simplified finite element models, they found that the residual stresses could be significant enough that the part could deform during the following machining operation to the point that material does not even engage with the tool. This leads to the part not meeting the design tolerances. However, this work was purely a modeling effort with no experimental validation.

The objective of the current work is to investigate the impact of residual stress on the geometric accuracy of parts produced using hybrid additive/subtractive manufacturing. Scan strategy, heat-treatment, and machining strategy are varied to quantify their impact on distortion. Stainless steel cylinders are created using powder bed fusion (PBF), then machined and the distortion from the machining operation is measured. Cylinders are produced using two different scan strategies that result in different thermal histories. Half of the cylinders are heat-treated to relieve the residual stress, while the other half are not, capturing one of the key differences between in-envelope and out-of-envelope hybrid strategies. The residual hoop and axial stress of select cylinders are measured using neutron diffraction and the as-produced surface is characterized using a laser confocal microscope. The inner diameter (ID) of each cylinder is machined to provide a reference surface that is measured with a coordinate measuring machine (CMM) before and after three different machining strategies are used to remove material from the outer diameter (OD). The results are then presented and discussed.

2. Experiment Setup

Figure 1 presents the experimental steps used in this study. First, cylinders are created using a LPBF process, then the inner and outer dimensions of those cylinders are measured using a CMM. Two identical sets of cylinders are created on two different substrates, one of which is used to study the as-produced residual stresses while the other is heat-treated to relieve the residual stresses. The dimensions of the heat-treated cylinders are re-measured using the CMM. Four cylinders are then removed from each substrate for post-process measurements: neutron diffraction to measure lattice spacing and from which residual stress is calculated, and laser confocal microscopy to characterize the roughness and profile

of the outer surface. The ID of each cylinder remaining on the substrates is machined to create a smooth reference surface, which is re-measured using the CMM. After this, material is removed from the outer perimeter using an end-mill and three different machining strategies. The cylinders are measured a final time using the CMM and the distortion from the OD machining is calculated. While this experimental method is akin to the out-of-envelope hybrid approach, the two different substrates (heat-treated and as-produced) are intended to study the anticipated difference between in-envelope and out-of-envelope hybrid strategies. The following sections describe each of these steps in greater detail before the results are presented and discussed.

	<u>Experiment Step</u>	<u>Description</u>
1)	Two separate builds are performed to create 12 cylinders on 2 different build plates (Referred to as Builds A and B).	Section 2.1
2)	The dimensions of each cylinder on both builds are measured using a CMM.	Section 2.2
3)	Heat-treat Build A to reduce residual stress.	Section 2.3
4)	Use a CMM to remeasure the dimensions of the cylinders of Build A.	Section 2.2
5)	Remove cylinders and sections of the build plate for additional measurements.	
6)	Characterize the outer surface of select cylinders.	Section 2.4
7)	Measure the residual stress in select cylinders using neutron diffraction.	Section 2.5
8)	Machine the ID of the remaining 8 cylinders on each plate.	Section 2.6
9)	Use a CMM to remeasure cylinders.	Section 2.2
10)	Machine the OD of the cylinders.	Section 2.7
11)	Use a CMM to remeasure cylinders.	Section 2.2

Figure 1 - Processing and measurement steps.

2.1. Cylinders Created using Powder Bed Fusion

Two substrates are machined from wrought American Iron and Steel Institute (AISI) 17-4 stainless steel. Each substrate is a 100 mm square and 12.7 mm thick with countersunk holes in each corner for fixturing. A single substrate is mounted on the build surface inside an EOSint M270 LPBF machine. EOS GP1 powder [10], which is equivalent in chemistry to AISI 17-4, is used to create 12 cylinders that are 12 mm tall and have nominal inner and outer diameters of 13 mm and 16 mm, respectively, as

shown in Figure 2. The powder used in this study has been recycled multiple times, but is sieved using a 65 μm mesh to remove any large particles from previous builds. Once the cylinders are built on the first substrate, it is removed from the machine so the second substrate can be mounted and the processes repeated.

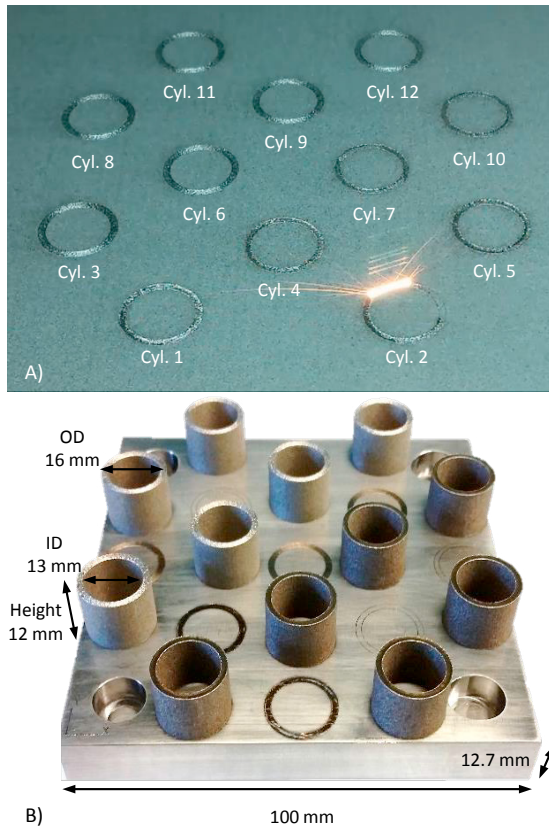


Figure 2 - A) Image acquired during the build and B) the final part. The different colors are a result of different thermal histories caused by different scan strategies.

Two different scan strategies are used to produce the 12 cylinders on each substrate, as illustrated in Figure 3. Half of the cylinders on each plate are created using the standard scan strategy, in which the laser scans back and forth in a raster pattern in pre-designated stripes that rotate by 67° each layer. The cylinders processed using the default scan strategy are in the lower right portion of the plate in Figure 2B and appear darker in color. The raster scans are performed with a laser power of 195 W traveling at a speed of 1 000 mm/s with 0.1 mm between adjacent raster scan tracks (hatch width). The width of the raster is 4 mm. The inner and outer perimeter of each cylinder is

scanned using a different set of contour processing conditions before and after the raster scan.

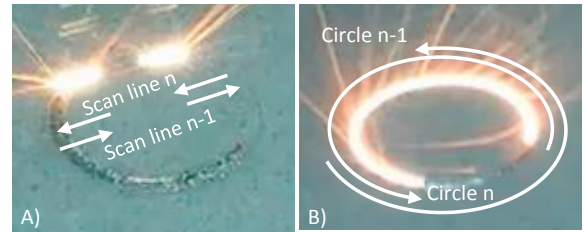


Figure 3 - The two scan strategies used in this study. A) Default raster strategy and B) concentric circles.

The other half of the cylinders are created by scanning the laser in 15 concentric circles. The laser power, speed, and hatch width are the same as the raster scan. In addition, the inner and outer perimeters of each cylinder are scanned according to the same contouring method. However, it should be noted that an error occurred while creating this scan pattern that caused the ID to be slightly smaller ($\approx 200 \mu\text{m}$) than the default strategy. This scan strategy is utilized to change the cooling rate and thermal history of the cylinders. Considering the scan speed and inner and outer diameters, each scan takes 40 ms to 50 ms to complete before the next laser scan begins to melt the adjacent powder and re-heat the newly solidified track. In contrast, a single default raster scan can be no longer than 9.3 mm in these parts and would take at most 9.3 ms to complete before the material is re-heated by the next adjacent scan track. Therefore, the default cylinders will experience higher temperatures for longer periods of time and will have slower cooling rates, potentially affecting the residual stress. The longer time spent at higher temperatures for the default scan strategy is evident by the darker color in those cylinders, located in the lower right portion of the substrate in Figure 2B. The darker color is a result of oxidation with the atmosphere in the LPBF processing chamber, which has an oxygen content between 0.5 % and 1.5 % during the process. Table 1 presents a summary of the PBF strategy used to create each cylinder and the subsequent processes and measurements performed on each cylinder. These processes and measurements are described in greater detail in the following sections.

Table 1 - Summary of the PBF strategy of each cylinder and the subsequent processing steps and measurements performed on each.

Build designation	Cylinder number	PBF scan strategy Raster or Concentric	Heat treated	Separated from build	Surface measured	Stress measured	OD machined (number of passes)	Distortion measured
A	1	R	X	X	X			
A	3	C	X	X	X			
A	10	R	X	X		X		
A	12	C	X	X		X		
A	2	R	X				X	X
A	4	R	X				X	X
A	5	R	X				X	X
A	6	C	X				X	X
A	7	R	X				X	X
A	8	C	X				X	X
A	9	C	X				X	X
A	11	C	X				X	X
B	1	R		X	X			
B	3	C		X	X			
B	10	R		X		X		
B	12	C		X		X		
B	2	R					X	X
B	4	R					X	X
B	5	R					X	X
B	6	C					X	X
B	7	R					X	X
B	8	C					X	X
B	9	C					X	X
B	11	C					X	X

2.2. CMM Measurements

The inner and outer diameters of each cylinder are measured with a CMM (International Organization for Standardization (ISO) 10360-2 maximum permissible error (MPE) of 5 μm) using a 2 mm diameter probe tip. The diameters are measured at various heights in

1 mm steps, beginning at a height of 2.5 mm from the top surface of the base plate, and concluding at a height of 11.5 mm, as illustrated in Figure 4. The diameter is calculated using eight measurements spread evenly around the circumference of the cylinder using the CMM inspection software. The variance is calculated and reported.

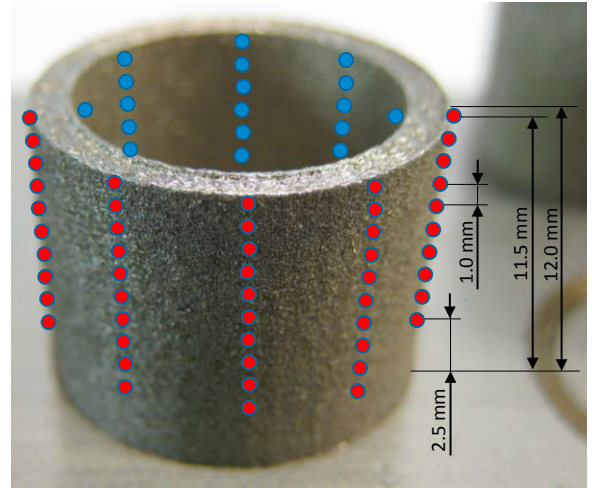


Figure 4 - Illustration of the CMM measurement locations. The ID (blue dots) and the OD (red dots) are measured at ten vertical locations using eight measurement points, equally spaced around the circumference.

2.3. Heat-Treatment

Build A is heat treated to relieve the residual stresses that are created during the PBF process. The part is cleaned using acetone and alcohol in an ultrasonic bath before heat treatment. It is then placed in a furnace and heated in a vacuum at a rate of 5 $^{\circ}\text{C}/\text{min}$ to reach a temperature of 400 $^{\circ}\text{C}$, where it is held for 20 min. This dwell is a necessary step to allow any existing carbonates to de-gas. Heating resumes at the same rate until a temperature of 650 $^{\circ}\text{C}$ is achieved and held for 1 h. The part is then allowed to cool in the furnace with He gas. In addition to relieving residual stress, the heat treat may also change the fraction of retained austenite, which is likely to occur in this material during PBF processing [11]. However, microstructure characterization is beyond the scope of the current study.

2.4. Characterization of the Outer Cylinder Surface

Two cylinders (Cylinders 1 and 3) and the plate material they are built on are removed from each of the substrates using electrical discharge machining (EDM) and their outer surfaces are characterized using a laser confocal microscope with a 10x objective. The microscope scans along the height of the cylinder adjacent to the build plate edge, allowing the side surface of the build plate to be included in the scan as a reference. The scanning is performed over an area 1.3 mm wide and 12.7 mm tall. Figure 5 presents images of Cylinders 1 and 3 from Build B with yellow rectangles indicating the approximate area scanned by the microscope.

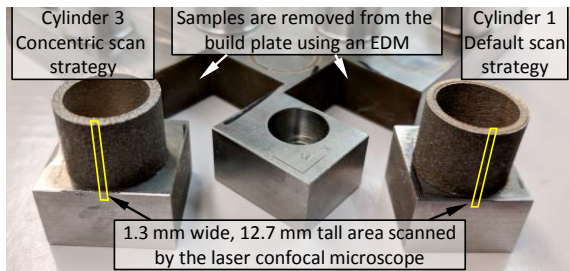


Figure 5 - The surface is characterized over an area on the outer diameter of select samples using a laser confocal microscope

2.5. Stress Measurement using Neutron Diffraction

Neutron diffraction is used for the non-destructive evaluation of the tri-axial stresses at the National Institute of Standards and Technology Center for Neutron Research (NCNR) using the stress diffractometer [12, 13]. Measurements are made on Cylinders 10 and 12 at 18 locations in the cylinder wall, as illustrated in Figure 6. The orientation and location dependent lattice spacings are measured from the neutron diffraction angle. The cross section of the diffracted beam and the neutron beam defines the gage volume, which in this work is approximately 0.5 mm wide, 2 mm tall, and 1 mm thick. Each measurement location averages the lattice spacing measured within this gage volume. The measurements are repeated on the opposite side of the cylinder to check for consistency. By assuming the radial stress through the cylinder is 0 MPa, and the material properties of 17-4 stainless steel, the average hoop and axial stresses at each measurement location are calculated. The

stresses are qualitatively verified by ensuring the axial and hoop directions are in equilibrium.

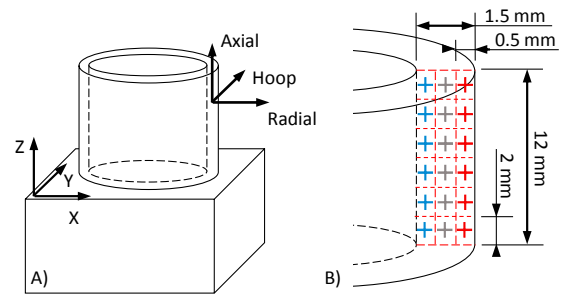


Figure 6 - Neutron diffraction measurement locations.

2.6. Inner Diameter Machining Operation

A small amount of material is removed from the inner diameter during this operation to create a smooth surface that can be reliably measured with the CMM, enabling the distortion resulting from the OD operation to be measured. The inner diameter of each cylinder remaining on the plate in Step 8 is machined based on the prior CMM measurements using a 10 mm diameter 3 flute end mill (SECO 910100R100-MEGA). The interior of the cylinder is machined from the top down using a cutting speed of 70 m/min, and a feed rate of 0.1 mm per tooth, in 64 μm steps, to a diameter of 13 mm, concluding at a height 0.5 mm above the substrate surface. Coolant is used. Although the cylinder ID is nominally 13 mm, the actual inner diameter is smaller than that, as will be shown later.

2.7. Outer Diameter Machining Operations

Figure 7 illustrates the OD machining operation. The same cutting tool from the ID machining operation is used to machine the OD of all cylinders. The location of each cut is based on location of each cylinder relative to the substrate as determined by the prior CMM measurement. The OD of each of the remaining eight cylinders is cut using climb milling at an axial depth of cut of 11.5 mm, a cutting speed of 70 m/min, and a feed rate of 0.1 mm per tooth. The tool engages each cylinder 20° offset from the +Y direction, makes one complete revolution then retracts. Coolant is used during this operation. Cylinders 2, 4, 6, and 8 are machined to an OD of 15 mm using a single pass. Cylinders 5 and 11 are machined to that diameter using two passes, with the

first taking the OD to 15.5 mm, and the second to a diameter of 15 mm. Cylinders 7 and 9 are machined to a diameter of 15.5 mm in a single pass. The variety of OD machining strategies allows the impact of the radial engagement to be investigated.

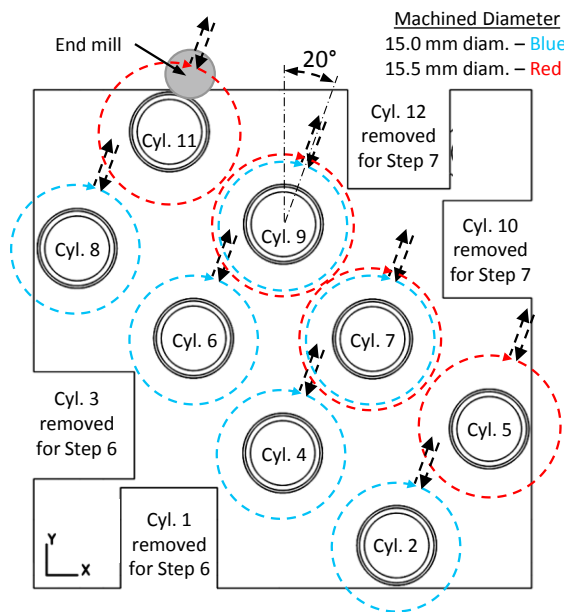


Figure 7 - The OD machining strategy for the remaining eight cylinders on each plate.

3. Results

The residual stress calculations from the neutron diffraction measurements of Cylinders 10 and 12 from Build B (as-produced) are presented in Figure 8. As shown in Figure 8A, hoop stress is primarily in tension near the outer circumference of the cylinder and primarily in compression near the inner circumference. The bottom of each cylinder is in tension because the cylinder is still attached to the substrate, which is preventing the cylinder from contracting. Qualitatively, these trends agree with the literature [9, 14]. The stress distribution is a result of the thermal processing: as the newly solidified material cools and contracts, it compresses the material below it, which in turn, resists the contraction of the new material. This explains the higher amounts of compression in the middle and tension in the top of each cylinder.

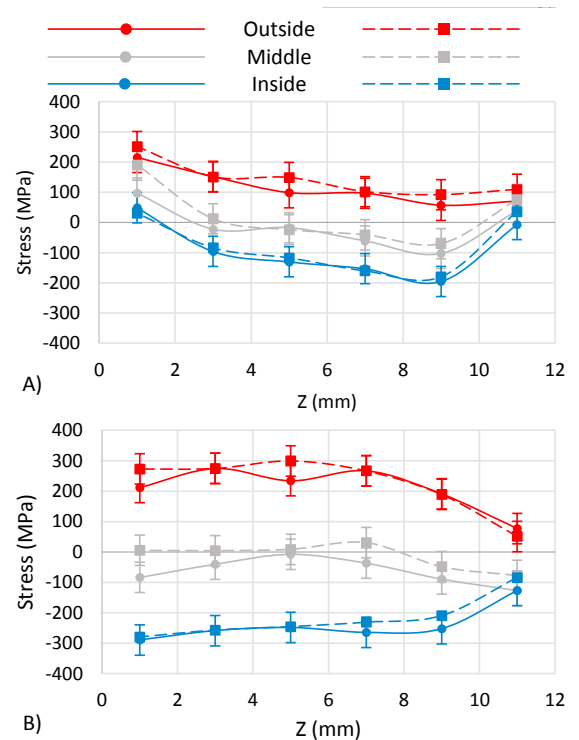


Figure 8 - Residual stress measurements of Cylinders 10 and 12 from the as-produced plate (Plate B). A) Hoop stress, B) axial stress. Error bars represent an estimated measurement uncertainty of 50 MPa.

Residual stress was not calculated from the neutron diffraction measurements of Cylinders 10 and 12 from Build A (heat-treated) because the heat treatment induced a phase change in the material that created a textured (multi-phase) material, which complicates the residual stress calculation. LPBF processed 17-4 stainless steel has been shown to be primarily metastable austenite [11] that easily transforms to martensite with subsequent heat treatments or cold work. The diffraction measurements confirm the presence of a second phase in the heat-treated cylinders. Unfortunately, the reduction in residual stress from the heat-treat cannot be confirmed.

Figure 9 shows a profile taken from the center of the optical scan for one of the cylinders in this study (Cylinder 1, Build A). From this profile, the arithmetic mean roughness, R_a , and root-mean-square roughness, R_q , are calculated based on the ISO 4287 standard using a digital gaussian filter with cutoff wavelength of 0.8 mm. Figure 9A shows that the surface is very rough (R_a of 16.5 μm and R_q of 19.7 μm) and consistent with the literature [15]. However, the form

error can be extracted from this measurement as shown in Figure 9B and shows that the cylinder does curve inward slightly. CMM measurements of the OD and ID have been acquired, however the rough surface makes the variance greater than the measured curvature.

Figure 10 shows a cylinder after each machining step. The surface resulting from the ID machining operation (Step 8) is smooth and shiny, as shown in Figure 10A, while the outer surface remains rough. This smooth surface is easy to measure with the CMM and is used as a reference surface to quantify the amount of distortion that results from the OD machining. The surface generated by the OD machining is shown in Figure 10B.

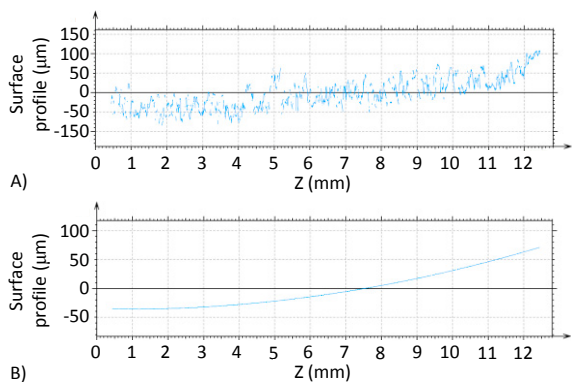


Figure 9 - Surface profile measurement of Cylinder 1 from Plate A. A) Profile with outliers removed, B) extracted form error.

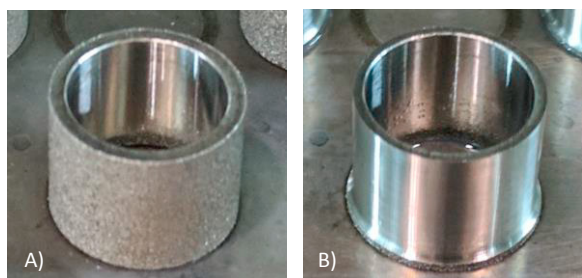


Figure 10 - Example cylinders after A) ID machining, Step 8 and B) OD machining, Step 10.

Figure 11 shows the CMM measurements of the inner diameter of each cylinder before and after OD machining. Measurements acquired before the operation are represented by dashed lines, and those acquired after are represented by solid lines. In all

cases the diameter decreases after the OD machining, with the greatest decrease near the top of the cylinders. The average concentricity of the ID and OD measurements is 15 µm.

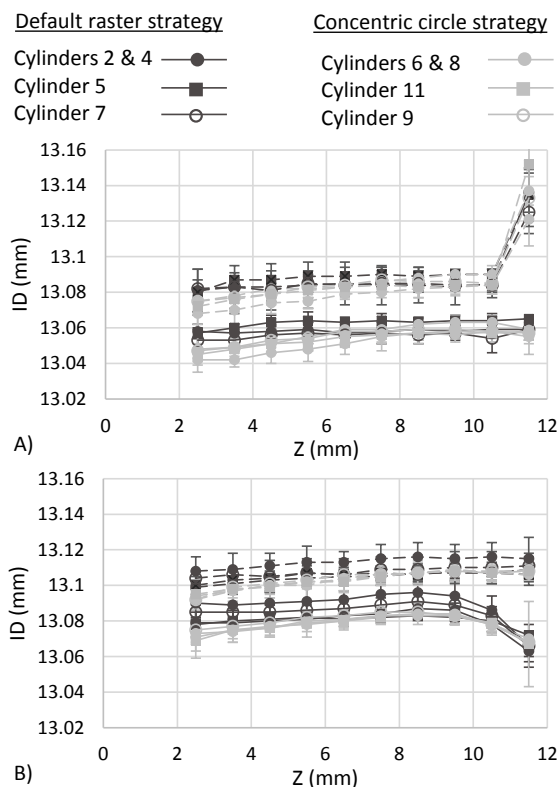


Figure 11 - ID measured before (dashed lines) and after (solid lines) the OD machining operation (Steps 9 and 11). A) Plate A, heat-treated B) Plate B, as-produced. Error bars represent the diameter measurement variance.

4. Discussion

There are several notable observations from these results. The first is that the cylinders distorted in the opposite direction than expected after the OD is machined. Figure 12 shows that based on the measured residual stress distribution in the part, the OD machining removed a majority of the material in tension. Removing this material would allow the remaining material that was primarily in compression to reach a new equilibrium, which would cause the cylinder to expand. However, the diameter measurements presented in Figure 11 clearly show that the cylinders contracted. There are three hypothesis that explain the decreasing diameter:

1. The residual stress measurements may be incorrect.
2. Machining may induce a phase-change in the material that affects residual stress and its equilibrium state.
3. The machining operation may induce compressive stresses that counteract the remaining stresses from the LPBF process, causing the cylinders to distort inward to reach a new equilibrium.

The first hypothesis seems unlikely considering the measured stress trends agree well with literature [9, 13]. The second hypothesis is far more likely, since it has been reported in the literature that the austenite in this AM material is meta-stable and can easily change to martensite through additional heat treatment or cold-work [11], both of which occur during metal cutting. The third possibility is just as likely as the second, since it is well known that metal cutting operations can induce high residual stresses in the workpiece [16].

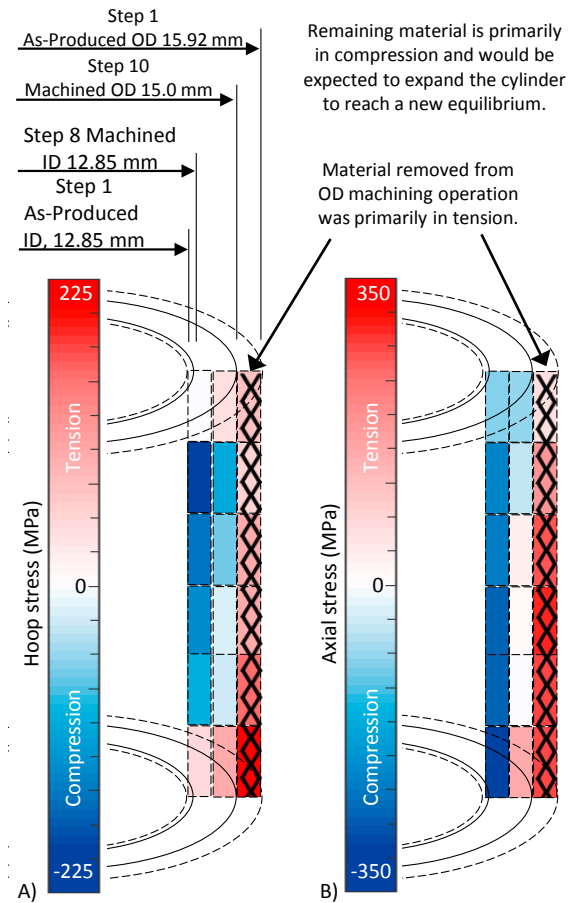


Figure 12 - Illustration of the assumed stress distribution and the anticipated impact of removing material from the OD on the ID measurements. A) Hoop stress, B) axial stress.

The second observation from the results in this study is that the chosen processing strategies used in this study have little to no significant impact on the amount of residual stress or distortion. Figure 13 shows that for every cylinder on each plate, the inner diameter decreased by 20 μm to 30 μm (from $Z = 2$ mm to $Z = 10$ mm), regardless of the processing conditions.

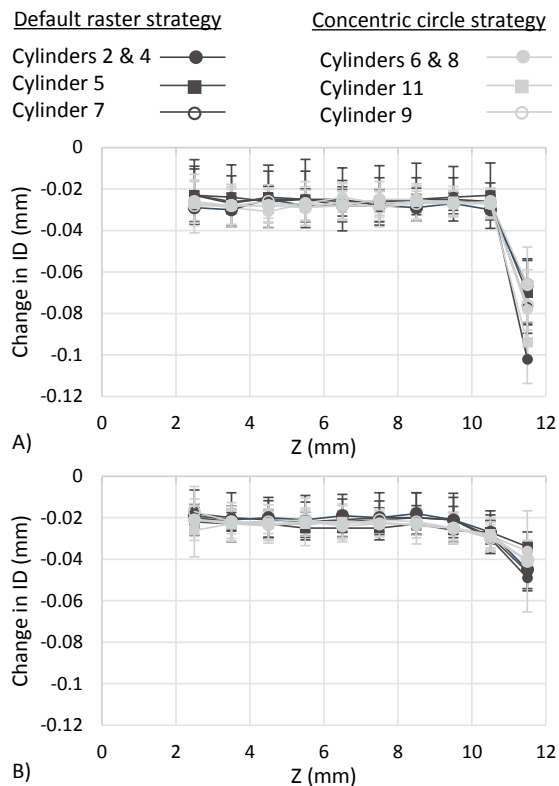


Figure 13 - Change in the inner diameter caused by machining the outer diameter. A) Plate A, heat-treated, B) Plate B, as-produced. Error bars represent the variance of the diameter calculations using the eight measurement points.

The difference between the two different scan strategies clearly has no effect on the residual stress or distortion. The residual stress measurements presented in Figure 8 show no difference between the as-produced and heat-treated cylinders. Furthermore, the gray and black lines in Figure 13 lie almost perfectly on top of each other. While scan strategy has been shown in the literature to impact distortion and residual stress [5], those instances are for larger scan areas and builds. However, the results for the cylinders in this current study are consistent with the trends reported by Dunbar et al. in their study using similarly sized cylinders and a similar LPBF process [14]. Their changes in scan strategy, albeit less drastic than those in the current study, had no significant impact on the measured distortion or simulated stresses.

The machining strategies used in the current study also appear to have no significant impact on distortion. Figure 13 shows that each cylinder within a certain build experienced the same amount of distortion due

to the OD machining operation, regardless of the radial engagement (approximately 0.5 mm in the even numbered cylinders, compared to approximately 0.25 mm in the odd numbered cylinders) or the number of cutting passes used to achieve the 15 mm OD (one pass for the even numbered cylinders vs. two passes for Cylinders 5 and 7). However, the tool geometry and cutting conditions were the same for all cases, so the observations regarding the impact on machining operations are limited to this study. It is expected that different tooling or cutting conditions would have a significant impact on the stresses induced in the cylinders and the resulting distortion.

The impact of the stress-relief heat treatment is less clear. Figure 13 shows that the heat-treated cylinders on Build A experienced slightly more distortion on average compared to Build B from $Z = 2.5$ mm to $Z = 8.5$ mm, $26 \mu\text{m}$ compared to $21 \mu\text{m}$, though this difference is within the variance of the measurement ($8 \mu\text{m}$). However, the trends near the top of the plate are significantly different. The heat-treated cylinders in Build A (Figure 13A) exhibit consistent distortion for most of the height, except for the last measurement location at 11.5 mm, which ranges between $66 \mu\text{m}$ and $102 \mu\text{m}$. In contrast, the distortion in the non-heat-treated cylinders on Build B (Figure 13B) begin to gradually increase at a height of $Z = 9.5$ mm, reaching maximum values ranging from $34 \mu\text{m}$ to $49 \mu\text{m}$ at the height of $Z = 11.5$ mm.

These distortion results suggest that the heat-treatment did alter the residual stresses in the cylinders (which unfortunately could not be confirmed using neutron diffraction due to the creation of a second phase). They also suggest that the machining process used in this study induced compressive stresses along the outer perimeter of the cylinders, supporting the second hypothesis presented earlier. If great enough, the induced machining stresses would cause the cylinders to contract despite the residual stresses generated by the LPBF process, which should have caused the cylinders to expand with the removal of the material along the outer perimeter. The distortion through the bulk of the as-produced cylinders in Build B (Figure 13B) is less than Build A because the compressive residual stresses from the LPBF process resisted the distortion induced by the OD machining operation compared to the heat-treated Build B. However, more work is required to better understand the stresses created in both AM and machining processes to fully understand these results and the

complexity of their interactions in hybrid additive/subtractive manufacturing.

5. Conclusions

This work investigated the part distortion that arises from the interaction of the multiple processes encountered during hybrid additive/subtractive manufacturing. Specifically, AM processes inherently create parts with high residual stresses that, in hybrid manufacturing, have portions of the material removed using machining operations. As a result, the stresses in the remaining material, and those potentially introduced by the machining process, must reach a new equilibrium, causing the part to distort. Cylinders that are 12 mm tall with a 16 mm outer diameter were created with powder bed fusion. The residual stresses in select as-produced cylinders were measured using neutron diffraction and the surfaces were characterized using a laser confocal microscope. After a reference surface was created on the inner diameter, the cylinders were then machined using a 3-flute end mill and the resulting distortion was measured using a CMM.

The residual stress in the as-produced cylinders measured using neutron diffraction qualitatively matches what is reported in the literature, where the outer material is primarily in tension and the inner material is primarily in compression. Based on the stress distribution in the cylinder, it was assumed that they would expand when a portion of the outer material was removed through machining, since the remaining material that was in compression would reach a new equilibrium. However, measurements revealed that the cylinders contracted during the outer diameter machining operation, suggesting that the chosen tooling and cutting conditions used in this study induced compressive stresses along the outer surface that counter-acted those remaining from the LPBF process. It is also possible that the machining operation induced a phase transformation of the metastable austenite, changing the stress balance. However, additional work is required to confirm these hypotheses and to better understand the complex interaction between additive and subtractive manufacturing processes.

Acknowledgements

The authors would like to thank the following individuals for their assistance. Kil-Won Moon

performed the heat treatments, Jared Tarr performed the EDM work, Jay Nanninga performed the CMM measurements, and Tyler Gervasio and Rick Lake were instrumental in the machining operations.

References

- [1] J. M. Flynn, A. Shokrani, S. T. Newman, and V. Dhokia, Hybrid additive and subtractive machine tools – Research and industrial developments. *International Journal of Machine Tools and Manufacture*, 101, (2016) 79–101.
- [2] J. Jones, P. McNutt, R. Tosi, C. Perry, and D. Wimpenny, Remanufacture of turbine blades by laser cladding, machining and in-process scanning in a single machine, *Proceedings of the 23rd Annual International Solid Freeform Fabrication Symposium*, (2012) 821–827.
- [3] G. Manogharan, R. Wysk, O. Harrysson, and R. Aman, AIMS–A Metal Additive-hybrid Manufacturing System: System Architecture and Attributes, *Procedia Manufacturing*, 1, (2015) 273–286.
- [4] F.-W. Goudsmit, G. Oosterhuis, E. Sluiter, and T. Peijnenburg, Typical requirements for precision mechanical parts and opportunities for additive manufacturing, *Proceedings of the ASPE Topical Meeting: Dimensional Accuracy and Surface Finish in Additive Manufacturing*, Berkeley, CA, (2014) 51–55.
- [5] P. Mercelis and J.-P. Kruth, Residual stresses in selective laser sintering and selective laser melting, *Rapid Prototyping Journal*, 12(5), (2006) 254–265.
- [6] E. R. Denlinger, J. Irwin, and P. Michaleris, Thermomechanical Modeling of Additive Manufacturing Large Parts, *Journal of Manufacturing Science and Engineering*, 136(6), (2014) 61007–61007.
- [7] E. R. Denlinger and P. Michaleris, Mitigation of distortion in large additive manufacturing parts, *Proceedings of the Institution of Mechanical Engineers, Part B: Journal of Engineering Manufacture*, 231(6), (2017) 983–993.
- [8] B. Lane, S. Moylan, and E. P. Whittenton, Post-process machining of additive manufactured stainless steel, *Proceedings of the 2015 ASPE Spring Topical Meeting: Achieving Precision Tolerances in Additive Manufacturing*, Raleigh, NC, (2015) 27–29.
- [9] K. Salonitis, L. D’Alvise, B. Schoinochoritis, and D. Chantzis, Additive manufacturing and post-processing simulation: laser cladding followed by high speed machining, *The International Journal of Advanced Manufacturing Technology*, 85(9-12), (2015) 2401–2411.
- [10] R. Stirling, EOS StainlessSteel GP1 for EOSINT M 270, EOS GmbH - Electro Optical Systems, Material Data Sheet, (2009).
- [11] S. Cheruvathur, E. A. Lass, and C. E. Campbell, Additive Manufacturing of 17-4 PH Stainless Steel: Post-processing Heat Treatment to Achieve Uniform Reproducible Microstructure, *JOM*, 68(3), (2016) 930–942.

- [12]P. Brand, H. Prask, and T. Gnaeupel-Herold, Residual stress measurements at the NIST reactor, *Physica B: Condensed Matter*, 241 (1997) 1244–1245.
- [13]T. Gnäupel-Herold, J. Slotwinski, and S. Moylan, Neutron measurements of stresses in a test artifact produced by laser-based additive manufacturing, presented at the AIP Conference Proceedings, 1581, (2014) 1205–1212.
- [14]A. J. Dunbar, E. R. Denlinger, M. F. Gouge, and P. Michaleris, Experimental validation of finite element modeling for laser powder bed fusion deformation, *Additive Manufacturing*, 12 (2016) 108–120.
- [15]A. Triantaphyllou, C.L. Giusca, G.D. Macaulay, F. Roerig, M. Hoebel, R.K. Leach, B. Tomita, K.A. Milne, Surface texture measurement for additive manufacturing, *Surface Topography: Metrology and Properties*, 3(2), (2015) 24002.
- [16]J. D. Thiele, S. N. Melkote, R. A. Peascoe, and T. R. Watkins, Effect of cutting-edge geometry and workpiece hardness on surface residual stresses in finish hard turning of AISI 52100 steel, *Journal of Manufacturing Science and Engineering*, 122(4), (200) 642–649.